Research Article | Vol. 24, No. 26 | 26 Dec 2016 | OPTICS EXPRESS 30139

Optics EXPRESS

Experimental study of wideband in-band full-duplex communication based on optical self-interference cancellation

YUNHAO ZHANG,[1] SHILIN XIAO,[1,*] YINGHONG YU,[1] CAO CHEN,[1] MEIHUA BI,[1,2] LING LIU,[1] LU ZHANG,[1,3] AND WEISHENG HU[1]

[1]*State Key Laboratory of Advanced Optical Communication System and Networks, Department of Electronic Engineering, Shanghai Jiao Tong University, Shanghai 200240, China*
[2]*College of Communication Engineering, Hangzhou Dianzi University, Xiasha Gaojiaoyuan 2rd Street, Hangzhou, Zhe Jiang province, 310018, China*
[3]*ONLab, School of ICT, The Royal Institute of Technology KTH, Kista, Stockholms 164 40, Sweden*
[*]*slxiao@sjtu.edu.cn*

Abstract: In this paper, we experimentally demonstrate and study a wideband in-band full-duplex (IBFD) wireless communication system based on optical self-interference cancellation (SIC). The optical SIC performances based on antennas for broadband IBFD are firstly evaluated within high frequency bands (> 10GHz). In this system, two electro-absorption-modulated lasers (EMLs) and a balanced photo-detector (BPD) are employed to remove the wideband self-interference within received wireless signal. By theoretical derivation and experimental verification, the impact factors of SIC are analyzed, especially for non-flatness wireless channel case. Experimental results show more than 30-dB cancellation depth in 100-MHz bandwidth with employment of horn antennas. Besides, IBFD transmission performance based on OFDM signals for different bandwidth with 11.15-GHz center frequency is also demonstrated, and ~52.2- dB•Hz$^{2/3}$ spurious-free dynamic range (SFDR) is obtained.

OCIS codes: (350.4010) Microwaves; (060.4510) Optical communications.

References and links

1. Z. Zhang, X. Chai, K. Long, A. V. Vasilakos, and L. Hanzo, "Full duplex techniques for 5G networks: Self-interference cancellation, protocol design, and relay selection," IEEE Commun. Mag. **53**(5), 128–137 (2015).
2. A. Sabharwal, P. Schniter, D. Guo, D. W. Bliss, S. Rangarajan, and R. Wichman, "In-band full-duplex wireless: Challenges and opportunities," IEEE J. Sel. Areas Comm. **32**(9), 1637–1652 (2014).
3. D. Kim, H. Lee, and D. Hong, "A survey of in-band full-duplex transmission: From the perspective of PHY and MAC layers," IEEE Comm. Surv. and Tutor. **17**(4), 2017–2046 (2015).
4. G. Liu, F. R. Yu, H. Ji, V. C. M. Leung, and X. Li, "In-band full-duplex relaying: A survey, research issues and challenges," IEEE Comm. Surv. and Tutor. **17**(2), 500–524 (2015).
5. P. A. Gamage, A. Nirmalathas, C. Lim, D. Novak, and R. Waterhouse, "Design and analysis of digitized RF-over-fiber links," J. Lightwave Technol. **27**(12), 2052–2061 (2009).
6. H. Kim, J. H. Cho, S. Kim, K. U. Song, H. Lee, J. Lee, B. Kim, Y. Oh, J. Lee, and S. Hwang, "Radio-over-fiber system for TDD-based OFDMA wireless communication systems," J. Lightwave Technol. **25**(11), 3419–3427 (2007).
7. Y. Xu, J. Yu, X. Li, J. Xiao, and G. K. Chang, "Demonstration of 120 Gbit/s full-duplex signal transmission over fiber-wireless-fiber network at W-band," in *Optical Fiber Communication Conference* (OFC, 2015) paper W4G.7.
8. M. Heino, D. Korpi, T. Huusari, E. A. Rodríguez, S. Venkatasubramanian, T. Riihonen, L. Anttila, C. Icheln, K. Haneda, R. Wichman, and M. Valkama, "Recent advances in antenna design and interference cancellation algorithms for in-band full duplex relays," IEEE Commun. Mag. **53**(5), 91–101 (2015).
9. M. Duarte, A. Sabharwal, V. Aggarwal, R. Jana, K. K. Ramakrishnan, C. W. Rice, and N. K. Shankaranarayanan, "Design and characterization of a full-duplex multi-antenna system for WiFi networks," IEEE Trans. Vehicular Technol. **63**(3), 1160–1177 (2014).
10. M. P. Chang, P. R. Prucnal, and Y. Deng, "Full-duplex spectrum sensing in cognitive radios using optical self-interference cancellation," in *Proceedings of IEEE 9th International Conference on Sensing Technology,* (ICST, 2015).

#280405 http://dx.doi.org/10.1364/OE.24.030139
Journal © 2016 Received 8 Nov 2016; revised 11 Dec 2016; accepted 16 Dec 2016; published 20 Dec 2016

11. P. Dat, A. Kanno, N. Yamamoto, and T. Kawanishi, "Full-duplex transmission of LTE-A carrier aggregation signal over a bidirectional seamless fiber-millimeter-wave system," J. Lightwave Technol. **34**(2), 691–700 (2016).
12. M. Duarte, "Full-duplex wireless: Design, implementation and characterization," Ph.D. dissertation, Rice University (2012).
13. A. Balatsoukas-Stimming, P. Belanovic, K. Alexandris, and A. Burg, "On self-interference suppression methods for low-complexity full-duplex MIMO," in *Proceedings of IEEE Asilomar Conference on Signals, Systems and Computers* (2013), pp. 992–997.
14. E. Foroozanfard, O. Franek, A. Tatomirescu, E. Tsakalaki, E. de Carvalho, and G. F. Pedersen, "Full-duplex MIMO system based on antenna cancellation technique," IEEE Electron. Lett. **50**(16), 1116–1117 (2014).
15. J. Suarez, K. Kravtsov, and P. R. Prucnal, "Incoherent method of optical interference cancellation for radio-frequency communications," IEEE J. Quantum Electron. **45**(4), 402–408 (2009).
16. M. Lu, M. Chang, Y. Deng, and P. R. Prucnal, "Performance comparison of optical interference cancellation system architectures," Appl. Opt. **52**(11), 2484–2493 (2013).
17. J. Bruno, M. Lu, Y. Deng, and P. Prucnal, "Broadband optical cosite interference cancellation," SPIE Opt. Eng. **52**(5), 053001 (2013).
18. Q. Zhou, H. Feng, G. Scott, and M. P. Fok, "Wideband co-site interference cancellation based on hybrid electrical and optical techniques," Opt. Lett. **39**(22), 6537–6540 (2014).
19. M. H. Huang, D. Zhu, and S. L. Pan, "Optical RF Interference Cancellation Based on a Dual-parallel Polarization Modulator," in *Asia Communications and Photonics Conference* (ACP, 2014), paper ATh1F.6.
20. Y. Zhang, S. Xiao, H. Feng, L. Zhang, Z. Zhou, and W. Hu, "Self-interference cancellation using dual-drive Mach-Zehnder modulator for in-band full-duplex radio-over-fiber system," Opt. Express **23**(26), 33205–33213 (2015).
21. Y. Xu, X. Li, J. Yu, and G. K. Chang, "Simple and reconfigured single-sideband OFDM RoF system," Opt. Express **24**(20), 22830–22835 (2016).

1. Introduction

Recently, in-band full-duplex (IBFD) communication has been gaining wide attention as an attractive trend for its supporting of bidirectional simultaneous radio frequency (RF) transmission within the same frequency band [1–4]. Compared to frequency-division duplex (FDD) and time-division duplex (TDD) mode [5–7], IBFD schemes significantly improve the spectrum efficiency and flexibility. Moreover, IBFD takes active effect in kinds of wireless systems, such as relay systems, ad hoc network, cognitive radios and radio-over-fiber (RoF) systems [8–11].

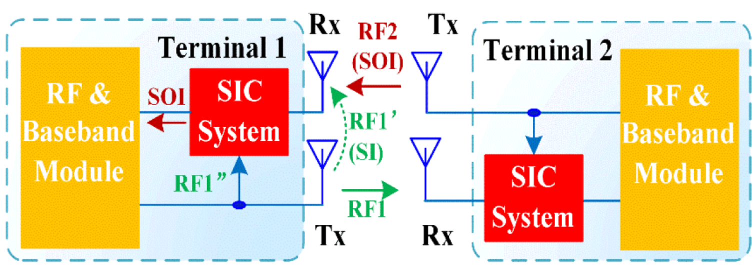

Fig. 1. Architecture of a basic IBFD end-to-end system. Tx: transmit antenna; Rx: receive antenna; SIC: self-interference cancellation

However, IBFD has not been widely used due to the challenges from the strong in-band self-interference (IBSI). Within the architecture of a basic IBFD end-to-end system as shown in Fig. 1, the receive antenna (Rx) of Terminal 1 gets to receive both RF2 and RF1', which represent transmit signal from Terminal 2 and IBSI signal from Terminal 1 itself, respectively. In this paper, RF2 is called signal of interest (SOI) and IBSI RF1' is simplified as self-interference (SI) towards Terminal 1. The SOI shares the same RF band with SI so that it cannot be removed by band pass filter or notch filter. The same case is also demonstrated on Terminal 2. In this case, self-interference cancellation (SIC) systems are investigated to enable IBFD mode to work, which are set following the Rx antennas to remove SI. The basic theory of SIC is to duplicate original transmit signal (RF1" in Fig. 1) into SIC system, and then to subtract SI after the amplitude and phase of the two signals are adjusted to be precisely matched. Although electronic SIC schemes have been widely investigated, the cancellation bandwidth typically achieve less than 40-MHz and the transmission frequency range are typically less than 5-GHz [12–14] due to bandwidth and linearity limitations of electrical devices. However, with the current tension both in wireless spectrum resource and capacity, developing higher frequency band and wider bandwidth is the obvious tendency for future mobile communication.

Optical or optical/electrical mixed SIC schemes have been proposed for larger IBFD bandwidth [15–20]. John Suarez *et al.* took advantage of positive and negative modulation of Mach-Zehnder modulators (MZMs) to remove SI, operated at 3-GHz band [15]. Qi Zhou *et al.* reported 30-dB cancellation depth over 5.5-GHz bandwidth by optical/electrical mixed SIC scheme, which is limited by the operation bandwidth of Balun and electro-absorption modulators (EAMs) employed [18]. Menghao Huang *et al.* demonstrated the SIC approach using dual-parallel polarization modulator (DP-PolM) to extend frequency band to 10 GHz [19]. But the IBFD transmission within higher frequency bands like X, Ku and K band were not given. To deal with this issue, we have proposed an optical SIC system based on dual-drive MZM (DD-MZM) to obtain higher frequency bands, and achieved up to 25-GHz frequency bands for IBFD [20]. However, the referenced optical or optical/electrical mixed SIC schemes are always simulated by cables and not tested in wireless channel, which limit the performance evaluation of SIC systems for IBFD communication.

In this paper, we experimentally demonstrate an IBFD system based on electro-absorption-modulated lasers (EMLs) and balanced photo-detector (BPD) with employment of broadband horn antennas, and study the SIC performance change caused by antennas and wireless channel. EMLs are employed in designed SIC system for their easy integration and miniaturization compared to MZMs. Based on this SIC system, IBFD operating frequency band can tend to 24-GHz. IBFD transmission ability of orthogonal frequency division multiplexing (OFDM) signals is investigated under different signal bandwidth and SOI/SI ratio, in order to test the system performance. Moreover, experimental results show a spurious-free dynamic range (SFDR) of 52.2 dB•$Hz^{2/3}$ of this SIC system, proving a good linearity for wideband IBFD communication.

2. Architecture and principle

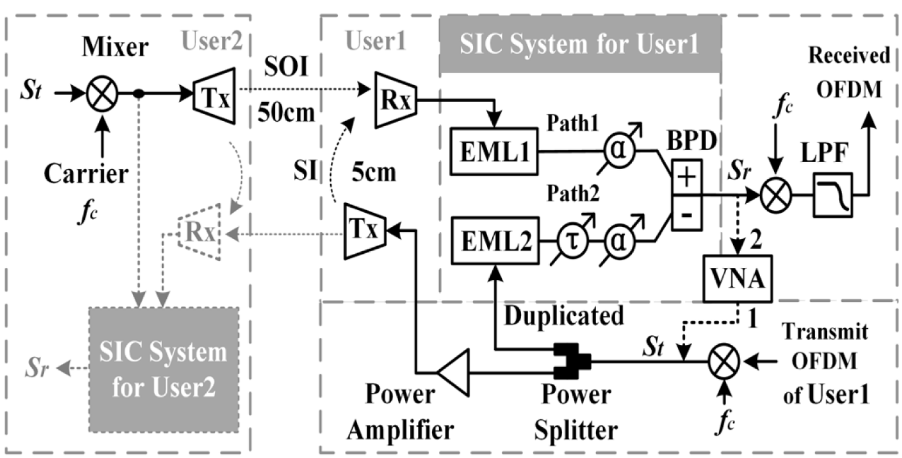

Fig. 2. Architecture of the demonstrated IBFD system and experimental setup. τ: optical time delay; α: optical attenuation; LPF: low-pass filter; f_c: RF carrier of transmit signals.

The architecture of the demonstrated IBFD system between two mobile users is depicted in Fig. 2. Each Tx and Rx antenna is configured to each user for transmitting and receiving wireless signals. The designed SIC system is set following Rx antenna, which consists of two EMLs, optical delay line, optical attenuators and one BPD. Transmit signal is duplicated into the SIC system before sent to Tx antenna. Due to the same principle and setup, receiver and SIC system are not configured in User2, but in User1 only. All the employed antennas are horn antennas with frequency range from 7 GHz to 25 GHz. Principles of the IBFD systems are stated as follows.

As for employed EMLs, their modulation curves include linear-slope-like region and zero-slope-like region, as shown in Fig. 3. Based on these curves, RF signals can be linearly modulated on optical carriers by setting proper bias voltage. In this paper, T_v is used to indicate the electric absorption function of EMLs. Optical output power of EML1 and EML2 are represented as I_1 and I_2 and shown in Eq. (1) and Eq. (2), respectively.

$$I_1 = I_{10}T_{v1}(V_{b1} + V_{SOI}(t) + V_{SI}(t)). \tag{1}$$

$$I_2 = I_{20}T_{v2}(V_{b2} + V_t(t)). \tag{2}$$

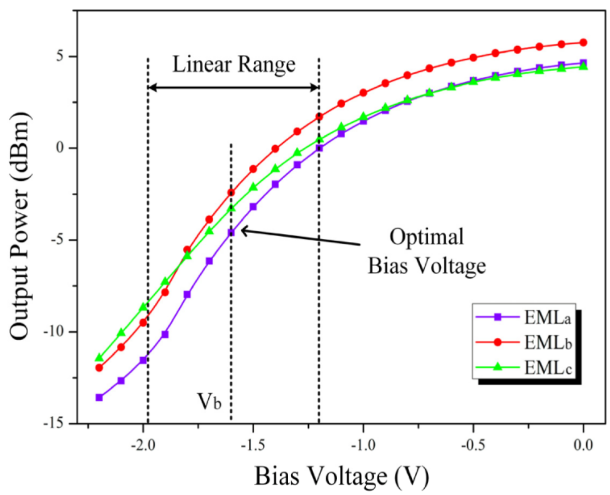

Fig. 3. Measured modulation curves of three tested EMLs

In Eq. (1) and Eq. (2), I_0 denotes output power of EML without electrical power input. As shown in Fig. 3, the modulation curves of three employed EMLs are measured. EMLa (red curve) and EMLb (purple curve) are chosen in our SIC system due to nearly the same electric absorption function (T_v), which means the same linear region and optimal bias voltage V_b. Nearby V_b, T_v is considered as linear function. Based on these, Eq. (1) and Eq. (2) can be refined as Eq. (3) and Eq. (4), respectively.

$$\begin{aligned} I_1 &= I_{10}T_v(V_b + V_{SOI}(t) + AV_{st}(t) * h(t)) \\ &= I_{10}T_v(V_b + V_{SOI}(t)) + I_{10}T_v(V_b + AV_{st}(t) * h(t)). \end{aligned} \tag{3}$$

$$I_2 = I_{20}T_v(V_b + A'V_{st}(t)). \tag{4}$$

$V_{st}(t)$ denotes transmitted RF signal, and $h(t)$ is the impulse response of wireless channel between Tx and Rx of User1. A and A' represent amplitude change within the signal transmission. After optical attenuation and optical delay, the output electrical signal of BPD $V_{sr}(t)$ is shown in Eq. (5), in which τ represents tunable time delay, α_1 and α_2 represent the tunable optical attenuation, and $\Re$ represents photo-electro response of BPD.

$$\begin{aligned} V_{sr}(t) &= \Re[\alpha_1 I_1(t) - \alpha_2 I_2(t-\tau)] \\ &= \Re[\alpha_1 I_{10}T_v(V_b + V_{SOI}(t)) + \alpha_1 I_{10}T_v(V_b + AV_{st}(t) * h(t)) - \alpha_2 I_{20}T_v(V_b + A'V_{st}(t-\tau))]. \end{aligned} \tag{5}$$

Optics EXPRESS

If the following equation holds

$$\alpha_1 I_{10} A T_v (V_b + V_{st}(t) * h(t)) = \alpha_2 I_{20} A' T_v (V_b + V_{st}(t-\tau)), \tag{6}$$

on condition that

$$\alpha_1 I_{10} A = \alpha_2 I_{20} A', \tag{7}$$

$$S_t(\omega) H(\omega) = S_t(\omega) e^{j\omega\tau}, \tag{8}$$

$$H(\omega) = e^{j\omega\tau}, \tag{9}$$

the Eq. (5) can be simplified as

$$V_{sr}(t) = \Re \alpha_1 I_{10} T_v (V_b + V_{SOI}(t)). \tag{10}$$

So the SOI is well recovered when $H(\omega) = e^{j\omega\tau}$ and $\alpha_1 I_{10} A = \alpha_2 I_{20} A'$, which means the wireless channel is amplitude-flat and phase-linear, as well as α_1 and α_2 are adjusted to proper value. In this ideal case, all the IBSI can be removed. However, due to the real non-flat wireless channel and the limitation of adjusted precision for optical attenuator and delay line, the IBSI cannot be removed totally. 30-dB cancellation depth is considered as good condition for broadband IBFD [15–20]. Moreover, the IBSI cancellation bandwidth is limited by channel response. The influence of wireless channel response on SIC performance is experimentally demonstrated and further discussed in Section 3.

3. Experimental results and discussion

3.1. SIC performance affected by channel response

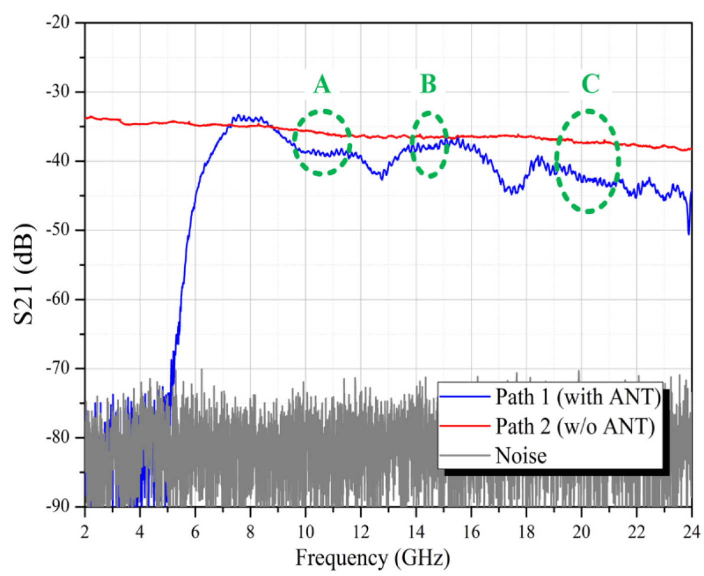

Fig. 4. S21 curves of Path1 (with antenna) and Path2 (without antenna)

To verify the theory analysis about SIC system mentioned above and further demonstrate IBFD transmission, we conduct the experiment, and the experimental setup is configured according to Fig. 2. The 10MHz~43.5-GHz Vector Network Analyzer (VNA) (KEYSIGHT N5224A) is employed to measure the S21 curve between $S_t(t)$ input port and $S_r(t)$ output port, as shown in Fig. 2. Swept single-tone RF signals from 2-GHz to 24-GHz are generated and

Optics EXPRESS

exported from Port1 of VNA. Firstly, we measure the S21 of Path1 (with antenna) and Path2 (without antenna), as depicted in Fig. 4. Due to transmitting through wireless channel, the response of Path1 is mainly affected by employed horn antennas. Then cancellation depth over working bands is calculated, the amount of which is determined by taking the difference between S21 curves of SIC system without and with cancellation. The cancellation depth curves describe cancellation effect of the SIC system, such as IBFD working bandwidth.

According to Eqs. (7)-(10), total IBSI can be removed if channel response of Path1 is amplitude-flat and phase-linear. Whereas, as shown in Fig. 4, S21 of Path1 (blue curve) is far from amplitude-flat in total bandwidth. Due to the channel selectivity of Path1, the two curves show relatively flatness only in several frequency bands such as A, B, and C regions circled. So we firstly investigate the cancellation depth in B-t-B case for suppressing the impact of antennas, so that to find the best cancellation performance of this SIC system. In this case, Tx and Rx of User1 are connected by a coaxial line, and cancellation depth is calculated, depicted as gray curve in Fig. 5. More than 25-dB cancellation depth over ~11-GHz broad bandwidth is achieved. And the cancellation depth of 20-dB can cover the frequency band up to 24-GHz. The cancellation curve shows the best cancellation performance this SIC system can reach.

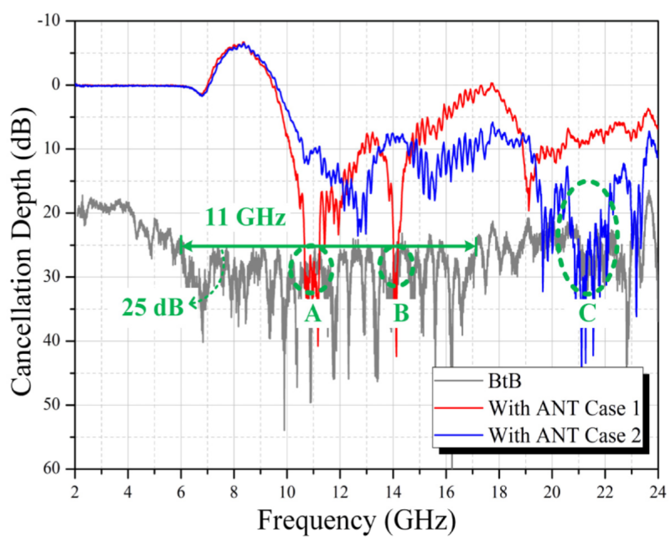

Fig. 5. Cancellation depth of SIC system without and with antenna

Then we measure the cancellation depth curves with antenna employed in Path1. Two cases with different time delays and attenuation adjustments are shown in Fig. 5 with the blue and red curves, respectively. In Case 1, cancellation depth in frequency region A and B is achieved close to that in B-t-B case. So do that in frequency region C in Case 2. Regions A, B and C in Fig. 5 are nearly one-to-one matched with that in Fig. 4, all of which show flat amplitude response. The experimental results prove that the flat amplitude of wireless channel response is essential to SIC performance, just as derived in Eq. (9). We can infer from the results that over some desired frequency regions within 0-24 GHz, IBFD mode can be supported if wireless channel response is comparatively flat in this regions. The IBFD transmission band is chosen according to cancellation depth curves in Fig. 5. The frequency region with higher cancellation depth such as Regions A, B and C can be chosen for IBFD communication due to better SIC performance.

Research Article Vol. 24, No. 26 | 26 Dec 2016 | OPTICS EXPRESS 30145

3.2. Broadband transmission in IBFD mode

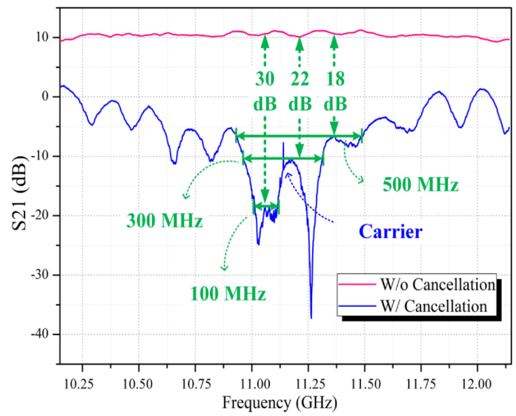

Fig. 6. S21 curves in transmission band before and after SI cancellation

Furthermore, the broadband OFDM-RF signal transmission in IBFD mode is experimentally demonstrated. According to the cancellation depth measurement in Fig. 5, frequency region A is selected as IBFD transmission band. Correspondingly, 11.15-GHz frequency is selected as center frequency. The measured S21 curves before and after cancellation near this region are shown in Fig. 6. About 30-dB cancellation depth is achieved over 100-MHz bandwidth. For 300-MHz and 500-MHz bandwidth, more than 22-dB and 18-dB cancellation depth are achieved respectively, which support broadband IBFD transmission. Moreover, the linearity of this SIC system is tested by measuring SFDR and third-order intercept point (IIP3). Two-tone signals at 11.10-GHz and 11.14-GHz are combined and injected into the SIC system. IIP3 is found as 22.6dBm, as shown in Fig. 7. Then SFDR is calculated by taking the difference of noise floor −68dBm/Hz and Pout −15.8dBm when the third order intermodulation (IMD3) is equal to noise floor, as a result of 52.2 dB•Hz$^{2/3}$. The SFDR is appeared to be limited by the high noise floor of −68 dBm/Hz. There are two main noise sources in the IBFD system. Firstly, the horn antennas employed in our experiment are wideband (7 GHz to 25 GHz) so that other RF signals of 7-25 GHz in the environment may be received as noise. Moreover, even though only one power amplifier (PA) is drawn in Fig. 2, actually there are PAs employed following receive antenna and BPD, which are not low-noise amplifiers. These PAs induce noises into the system.

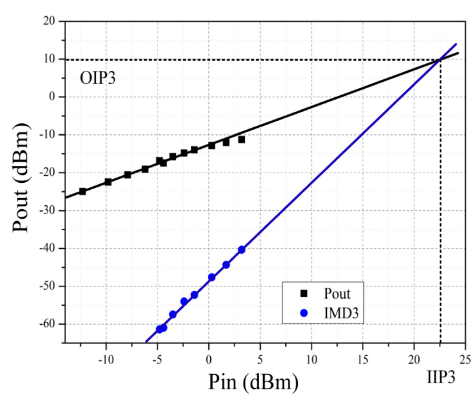

Fig. 7. IIP3 measurement of the SIC system

To emulate the real IBFD transmission, the analog OFDM signals in this 11.15-GHz RF band are selected since the OFDM has been used as air interface waveform technology in 4G and the foundation of next generation technologies [21]. VNA is now disconnected from the SIC system. The transmitted 16-Quadrature Amplitude Modulation (16-QAM) OFDM signals of User1 and User2 are generated offline by an arbitrary waveform generator (AWG, Tektronix AWG7122C) and both mixed with 11.15-GHz carrier frequency fc generated by the microwave source. After SIC, received signal is photo-detected. Cancellation on frequency domain is observed first by an RF spectrum analyzer (ROHDE & SCHWARZ FSUP, 20 Hz~50 GHz) employed following BPD.

Electrical spectra of received signals before and after cancellation are shown in Fig. 8. In this case both SOI and SI signals occupy 100-MHz RF bandwidth with 195.31-Mbps data rate. Before cancellation, the SOI is totally buried by the IBSI, and the spectrum is shown by the green curve in Fig. 8. Because the power of SI is higher than SOI, the observed spectrum of SI + SOI is the same as that of SI alone. So the green curve can represent both the spectrum of SI and SI + SOI. We close the SOI to observe the cancellation of SI. After cancellation, the SI signal power is reduced by 28 dB, shown as the brown curve in Fig. 8. Then the SOI is open and the blue spectrum depicts the SOI with SI cancelled. The effect of this removing is verified by constellation diagram observation in time domain. Received signals are sampled by a real-time oscilloscope (LeCroy SDA845Zi-A) and processed offline to observe the recovery of OFDM-RF signals from User2. Figure 8 (i) depicts the constellation diagram of SOI buried by SI. After SIC the constellation diagram is well-recovered obviously with 8.675% EVM, as shown in Fig. 8 (ii). The results prove the IBFD OFDM transmission between the two users.

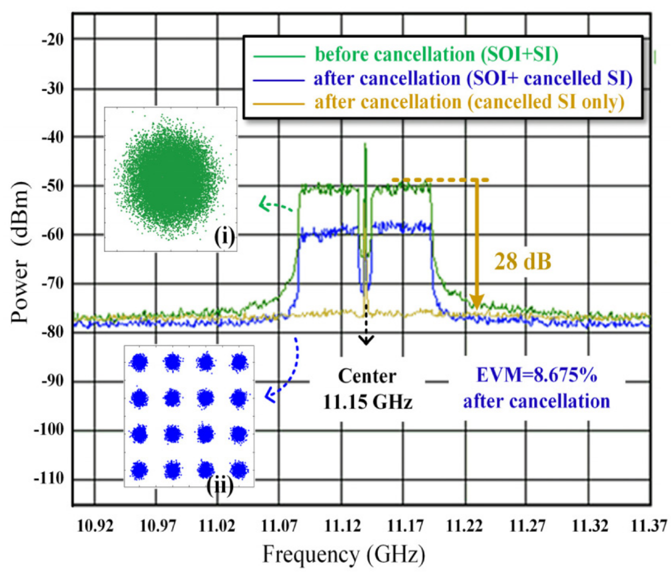

Fig. 8. Spectra and constellation diagrams of received Sr(t) before and after cancellation

Optics EXPRESS

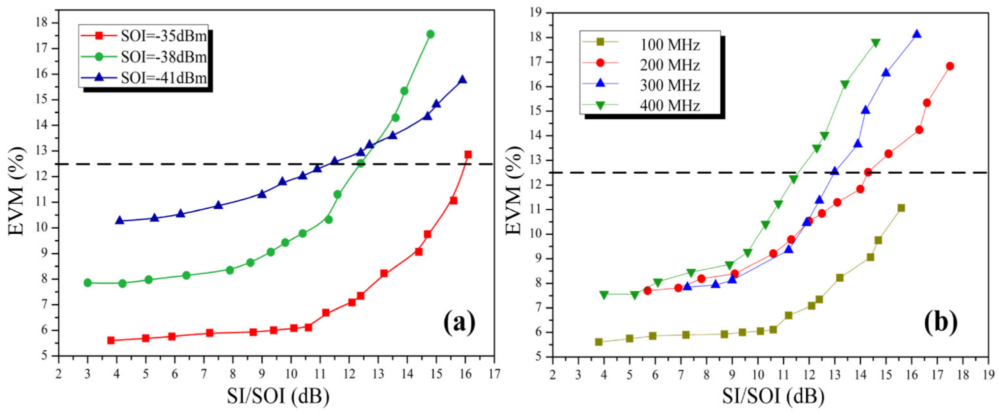

Figures 9. EVMs with different SI/SOI ratio under different (a) SOI values and (b) signal bandwidth

Moreover, we also evaluate the effect of relevant parameters on EVMs, which would influence the IBFD transmission performance. First, the SI/SOI ratio is employed to show how much interference SI takes on SOI. The values of SI and SOI are measured by the RF analyzer at the point after LPF in Fig. 2. When SI or SOI is measured, the other's signal source is closed at the AWG. Figure 9(a) depicts the EVMs versus SI/SOI ratio for different SOI values within 100-MHz transmission bandwidth. For all the three SOI investigated values, the more the SOI ratio, the lager EVMs is measured out, especially for more than ~11 dB SOI/SI ratio. We define SI' as the SI after cancellation. When SI/SOI is lower than 11 dB, the SI'/SOI is lower than −20 dB with the cancellation of SI ~30 dB. In this case SI' is not the dominant interference, but system noises mainly influence EVM values. Thus the EVM performance is tend to a limitation even though SI/SOI is smaller and smaller. We can also observe from the Fig. 9(b) that the SI/SOI when EVM rises more rapidly is lower than 11 dB in larger bandwidth cases because the cancellation depth is smaller than that in 100-MHz case. Moreover, the smaller the set SOI, the worse EVMs are achieved in general. For SOI of −35 dBm, SOI can be recovered at 12.5% EVM under about 16-dB SI/SOI circumstance. The EVM values of the case without antenna employed (BtB) is nearly identical to the case with antenna, because the cancellation curves of the two cases in Region A are overlapping as shown in Fig. 5.

Then EVMs versus SI/SOI ratio under different signal bandwidths are shown in Fig. 9(b), in which case SOI is set −35 dBm. Corresponding to cancellation depth within different bandwidth as shown in Fig. 6, for the larger the signal bandwidth case, the worse EVMs are achieved. As the similar trend in Fig. 9(a), larger SI/SOI ratio results in larger EVMs, which is obviously observed when SI/SOI is more than 11 dB. There is EVM jumping from the case of 100 MHz to the case set of 200, 300 and 400 MHz observed in Fig. 9(b). This appearance is corresponding to the cancellation depth of the SIC system. According to Fig. 6, the cancellation depth within the range of 100MHz achieves 30-dB, apparently larger than those within 300 MHz and 500 MHz. So the cancellation performance in 100 MHz bandwidth appears much better than those in 200, 300 and 400 MHz cases.

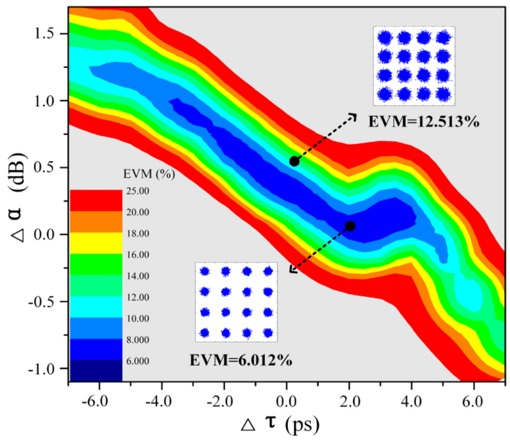

Fig. 10. EVMs with the bias of optical time delay and attenuation

For all the experimental results shown above, the EVMs are measured when cancellation depth is in the best condition, which means the optical time delay τ and attenuation α of Path 2 are adjusted to appropriate value for the minimum EVM. However, in practical IBFD system, the two parameters may not be adjusted in time if the environment have a quick micro disturbance. In this case, in order to investigate the adjustment redundancy of α and τ, we conduct the experiment with the bias of α and τ in Path 2 when SOI is set −35 dBm and signal bandwidth is set 100 MHz. Figure 10 depicts the EVMs with the bias of α and τ. We observe that with the △τ from −4 to 4 ps increase, the reducing of △α can keep EVMs at low value, under 8%. For a certain △τ within −6 to 5 ps region, there is about 0.4-dB △α jitter budget if EVMs is needed under 12.5%. The results show disturbance budget of the SIC system, which means IBFD is supported even if time delay and attenuation are not accurately adjusted to optimal state.

4. Conclusion

In this paper, by using the antennas, we have experimentally demonstrated and studied an IBFD wireless transmission. The IBFD transmission relies on the SIC system, which is based on EMLs and BPD to cancel the strong signal from transmit antenna of itself. Channel response between two antennas is proved to be the key element for impacting SIC performance. IBFD based on broadband OFDM signals in >10-GHz high frequency band is also shown with the SIC system employed. Cancellation performances are investigated under different signal bandwidths. At most 400-MHz IBFD transmission is supported, in which the successful recovery ~781-Mbps of 16-QAM OFDM is obtained. Moreover, by measuring SFDR of 52.2 dB•Hz$^{2/3}$, we also verify that this SIC system have a good linearity.

Acknowledgment

The work was jointly supported by the National Nature Science Fund of China (No.61271216, No. 61501157, No. 61221001, No.61090393 and No.61433009), the National “973” Project of China (No. 2010CB328205, No.2010CB328204 and No. 2012CB315602) and Natural Science Foundation of Zhejiang Province, China (Grant No. LQ16F050004).